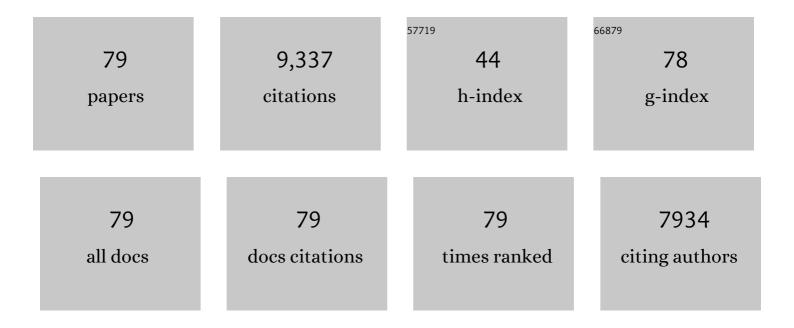
List of Publications by Year in descending order

Source: https://exaly.com/author-pdf/4496456/publications.pdf Version: 2024-02-01



SHUELI

#	Article	IF	CITATIONS
1	Semiconductor heterojunction photocatalysts: design, construction, and photocatalytic performances. Chemical Society Reviews, 2014, 43, 5234.	18.7	3,257
2	Photocatalytic degradation of tetracycline antibiotic by a novel Bi2Sn2O7/Bi2MoO6 S-scheme heterojunction: Performance, mechanism insight and toxicity assessment. Chemical Engineering Journal, 2022, 429, 132519.	6.6	279
3	Facile construction of novel Bi2WO6/Ta3N5 Z-scheme heterojunction nanofibers for efficient degradation of harmful pharmaceutical pollutants. Chemical Engineering Journal, 2020, 402, 126165.	6.6	277
4	Photocatalytic degradation of antibiotics using a novel Ag/Ag2S/Bi2MoO6 plasmonic p-n heterojunction photocatalyst: Mineralization activity, degradation pathways and boosted charge separation mechanism. Chemical Engineering Journal, 2021, 415, 128991.	6.6	253
5	Rationally designed Ta3N5/BiOCl S-scheme heterojunction with oxygen vacancies for elimination of tetracycline antibiotic and Cr(VI): Performance, toxicity evaluation and mechanism insight. Journal of Materials Science and Technology, 2022, 123, 177-190.	5.6	232
6	In situ construction of WO3 nanoparticles decorated Bi2MoO6 microspheres for boosting photocatalytic degradation of refractory pollutants. Journal of Colloid and Interface Science, 2019, 556, 335-344.	5.0	219
7	<i>In situ</i> construction of a C ₃ N ₅ nanosheet/Bi ₂ WO ₆ nanodot S-scheme heterojunction with enhanced structural defects for the efficient photocatalytic removal of tetracycline and Cr(<scp>vi</scp>). Inorganic Chemistry Frontiers, 2022, 9, 2479-2497.	3.0	217
8	Facile fabrication of TaON/Bi2MoO6 core–shell S-scheme heterojunction nanofibers for boosting visible-light catalytic levofloxacin degradation and Cr(VI) reduction. Chemical Engineering Journal, 2022, 428, 131158.	6.6	203
9	Synthesis of Ta ₃ N ₅ /Bi ₂ MoO ₆ core–shell fiber-shaped heterojunctions as efficient and easily recyclable photocatalysts. Environmental Science: Nano, 2017, 4, 1155-1167.	2.2	180
10	Facile construction of novel organic–inorganic tetra (4-carboxyphenyl) porphyrin/Bi2MoO6 heterojunction for tetracycline degradation: Performance, degradation pathways, intermediate toxicity analysis and mechanism insight. Journal of Colloid and Interface Science, 2022, 605, 727-740.	5.0	176
11	Facile synthesis of cerium oxide nanoparticles decorated flower-like bismuth molybdate for enhanced photocatalytic activity toward organic pollutant degradation. Journal of Colloid and Interface Science, 2018, 530, 171-178.	5.0	167
12	Constructing Cd0.5Zn0.5S/Bi2WO6 S-scheme heterojunction for boosted photocatalytic antibiotic oxidation and Cr(VI) reduction. , 2023, 2, 100073.		158
13	Impacts of energy consumption structure, energy intensity, economic growth, urbanization on PM2.5 concentrations in countries globally. Applied Energy, 2018, 230, 94-105.	5.1	155
14	Designing oxygen vacancy mediated bismuth molybdate (Bi2MoO6)/N-rich carbon nitride (C3N5) S-scheme heterojunctions for boosted photocatalytic removal of tetracycline antibiotic and Cr(VI): Intermediate toxicity and mechanism insight. Journal of Colloid and Interface Science, 2022, 624, 219-232.	5.0	155
15	Facile synthesis of flower-like Ag 3 VO 4 /Bi 2 WO 6 heterojunction with enhanced visible-light photocatalytic activity. Journal of Colloid and Interface Science, 2017, 501, 156-163.	5.0	152
16	Coupling analysis of urbanization and energy-environment efficiency: Evidence from Guangdong province. Applied Energy, 2019, 254, 113650.	5.1	137
17	Rationally designed tetra (4-carboxyphenyl) porphyrin/graphene quantum dots/bismuth molybdate Z-scheme heterojunction for tetracycline degradation and Cr(VI) reduction: Performance, mechanism, intermediate toxicity appraisement. Journal of Colloid and Interface Science, 2022, 619, 307-321.	5.0	135
18	Strategizing the relation between urbanization and air pollution: Empirical evidence from global countries. Journal of Cleaner Production, 2020, 243, 118615.	4.6	132

#	Article	IF	CITATIONS
19	A novel 3D Z-scheme heterojunction photocatalyst: Ag ₆ Si ₂ O ₇ anchored on flower-like Bi ₂ WO ₆ and its excellent photocatalytic performance for the degradation of toxic pharmaceutical antibiotics. Inorganic Chemistry Frontiers, 2020, 7, 529-541.	3.0	121
20	Constructing a plasmonic p-n heterojunction photocatalyst of 3D Ag/Ag6Si2O7/Bi2MoO6 for efficiently removing broad-spectrum antibiotics. Separation and Purification Technology, 2021, 254, 117579.	3.9	119
21	Facile synthesis of Fe 2 O 3 nanoparticles anchored on Bi 2 MoO 6 microflowers with improved visible light photocatalytic activity. Journal of Colloid and Interface Science, 2017, 497, 93-101.	5.0	96
22	Hierarchical hollow MnO2 nanofibers with enhanced supercapacitor performance. Journal of Colloid and Interface Science, 2018, 513, 448-454.	5.0	93
23	Facile construction of flower-like bismuth oxybromide/bismuth oxide formate p-n heterojunctions with significantly enhanced photocatalytic performance under visible light. Journal of Colloid and Interface Science, 2019, 548, 12-19.	5.0	92
24	Examining the effects of socioeconomic development on China's carbon productivity: A panel data analysis. Science of the Total Environment, 2019, 659, 681-690.	3.9	92
25	In situ anion exchange strategy to construct flower-like BiOCl/BiOCOOH p-n heterojunctions for efficiently photocatalytic removal of aqueous toxic pollutants under solar irradiation. Journal of Alloys and Compounds, 2019, 781, 582-588.	2.8	91
26	Hierarchical architectures of bismuth molybdate nanosheets onto nickel titanate nanofibers: Facile synthesis and efficient photocatalytic removal of tetracycline hydrochloride. Journal of Colloid and Interface Science, 2018, 521, 42-49.	5.0	90
27	Facile Preparation of a Novel Bi2WO6/Calcined Mussel Shell Composite Photocatalyst with Enhanced Photocatalytic Performance. Catalysts, 2020, 10, 1166.	1.6	89
28	In situ construction of heterostructured bimetallic sulfide/phosphide with rich interfaces for high-performance aqueous Zn-ion batteries. Science China Materials, 2022, 65, 356-363.	3.5	82
29	Synthesis of flower-like Ag2O/BiOCOOH p-n heterojunction with enhanced visible light photocatalytic activity. Applied Surface Science, 2017, 397, 95-103.	3.1	81
30	Flower-like Bi ₂ S ₃ /Bi ₂ MoO ₆ heterojunction superstructures with enhanced visible-light-driven photocatalytic activity. RSC Advances, 2015, 5, 75081-75088.	1.7	78
31	Evaluating the energy-environment efficiency and its determinants in Guangdong using a slack-based measure with environmental undesirable outputs and panel data model. Science of the Total Environment, 2019, 663, 878-888.	3.9	77
32	Surface decoration of Bi2WO6 superstructures with Bi2O3 nanoparticles: an efficient method to improve visible-light-driven photocatalytic activity. CrystEngComm, 2013, 15, 9011.	1.3	75
33	Examining the spatially varying effects of factors on PM2.5 concentrations in Chinese cities using geographically weighted regression modeling. Environmental Pollution, 2019, 248, 792-803.	3.7	70
34	What are the impacts of demographic structure on CO2 emissions? A regional analysis in China via heterogeneous panel estimates. Science of the Total Environment, 2019, 650, 2021-2031.	3.9	69
35	Examining the Impacts of Urban Form on Air Pollution in Developing Countries: A Case Study of China's Megacities. International Journal of Environmental Research and Public Health, 2018, 15, 1565.	1.2	68
36	Socioeconomic driving forces and scenario simulation of CO2 emissions for a fast-developing region in China. Journal of Cleaner Production, 2019, 216, 217-229.	4.6	66

#	Article	IF	CITATIONS
37	Does modernization affect carbon dioxide emissions? A panel data analysis. Science of the Total Environment, 2019, 663, 426-435.	3.9	66
38	Construction of fiber-shaped silver oxide/tantalum nitride p-n heterojunctions as highly efficient visible-light-driven photocatalysts. Journal of Colloid and Interface Science, 2017, 504, 561-569.	5.0	64
39	Dose urban landscape pattern affect CO2 emission efficiency? Empirical evidence from megacities in China. Journal of Cleaner Production, 2018, 203, 164-178.	4.6	53
40	Ta3N5-Pt nonwoven cloth with hierarchical nanopores as efficient and easily recyclable macroscale photocatalysts. Scientific Reports, 2014, 4, 3978.	1.6	52
41	Plasmonic p-n heterojunction of Ag/Ag2S/Ag2MoO4 with enhanced Vis-NIR photocatalytic activity for purifying wastewater. Separation and Purification Technology, 2020, 251, 117347.	3.9	52
42	Hierarchical MnO2 nanosheets on electrospun NiCo2O4 nanotubes as electrode materials for high rate capability and excellent cycling stability supercapacitors. Journal of Alloys and Compounds, 2016, 678, 120-125.	2.8	51
43	Photocatalytic reduction of CO2 and degradation of Bisphenol-S by g-C3N4/Cu2O@Cu S-scheme heterojunction: Study on the photocatalytic performance and mechanism insight. Carbon, 2022, 193, 272-284.	5.4	51
44	Enhanced photocatalytic conversion of NOx with satisfactory selectivity of 3D-2D Bi4O5Br2-GO hierarchical structures via a facile microwave-assisted preparation. Separation and Purification Technology, 2021, 266, 118237.	3.9	49
45	Rationally designed S-scheme heterojunction of C3N4/Bi2MoO6/carbon fiber cloth as a recyclable, macroscopic and efficient photocatalyst for wastewater treatment. Chemical Engineering Journal, 2022, 445, 136703.	6.6	46
46	A Novel Heterostructure of BiOI Nanosheets Anchored onto MWCNTs with Excellent Visible-Light Photocatalytic Activity. Nanomaterials, 2017, 7, 22.	1.9	45
47	Regional inequality, spatial spillover effects, and the factors influencing city-level energy-related carbon emissions in China. Journal of Chinese Geography, 2018, 28, 495-513.	1.5	44
48	<i>In situ</i> crystallization and growth of TiO ₂ nanospheres between MXene layers for improved adsorption and visible light photocatalysis. Catalysis Science and Technology, 2021, 11, 3834-3844.	2.1	44
49	Synthesis of n -type TaON microspheres decorated by p -type Ag 2 O with enhanced visible light photocatalytic activity. Molecular Catalysis, 2017, 435, 135-143.	1.0	40
50	Highly enhanced photodegradation of emerging pollutants by Ag/AgCl/Ta2O5â^'x mesocrystals. Separation and Purification Technology, 2021, 279, 119733.	3.9	39
51	Facile synthesis of hierarchical mesoporous NiCo2O4 nanoflowers with large specific surface area for high-performance supercapacitors. Materials Letters, 2017, 187, 129-132.	1.3	37
52	Ag3VO4 Nanoparticles Decorated Bi2O2CO3 Micro-Flowers: An Efficient Visible-Light-Driven Photocatalyst for the Removal of Toxic Contaminants. Frontiers in Chemistry, 2018, 6, 255.	1.8	37
53	BiOCOOH Microflowers Decorated with Ag/Ag2CrO4 Nanoparticles as Highly Efficient Photocatalyst for the Treatment of Toxic Wastewater. Catalysts, 2020, 10, 93.	1.6	30
54	Integration of plasmonic effect and S-scheme heterojunction into gold decorated carbon nitride/cuprous oxide catalyst for photocatalysis. Journal of Cleaner Production, 2022, 360, 131948.	4.6	29

#	Article	IF	CITATIONS
55	Construction of a novel ternary Ag/AgBr/Ag2WO4 composite for efficient photocatalytic removal of Rhodamine B dye and tetracycline hydrochloride antibiotic. Materials Letters, 2018, 224, 29-32.	1.3	28
56	Photocatalytic oxidation of tetracycline, reduction of hexavalent chromium and hydrogen evolution by Cu2O/g-C3N4 S-scheme photocatalyst: Performance and mechanism insight. Applied Surface Science, 2022, 592, 153309.	3.1	27
57	Magnetically recyclable and remarkably efficient visible-light-driven photocatalytic hexavalent chromium removal based on plasmonic biochar/bismuth/ferroferric oxide heterojunction. Journal of Colloid and Interface Science, 2021, 590, 424-435.	5.0	26
58	Synthesis of flower-like Ta3N5-Au heterojunction with enhanced visible light photocatalytic activity. Journal of Alloys and Compounds, 2017, 695, 1137-1144.	2.8	26
59	One-pot solvothermal synthesis of Ag nanoparticles decorated BiOCOOH microflowers with enhanced visible light activity. Materials Letters, 2017, 196, 343-346.	1.3	25
60	Hierarchical assembly of manganese dioxide nanosheets on one-dimensional titanium nitride nanofibers for high-performance supercapacitors. Journal of Colloid and Interface Science, 2019, 552, 712-718.	5.0	25
61	Constructing an ohmic junction of copper@ cuprous oxide nanocomposite with plasmonic enhancement for photocatalysis. Journal of Colloid and Interface Science, 2022, 616, 163-176.	5.0	25
62	Visible-light photocatalytic tetracycline degradation over nanodots-assembled N-ZrO2â^'x nanostructures: Performance, degradation pathways and mechanistic insight. Journal of Alloys and Compounds, 2022, 895, 162582.	2.8	24
63	MWCNTs/BiOCOOH composites with improved sunlight photocatalytic activity. Materials Letters, 2017, 191, 157-160.	1.3	22
64	Ag ₂ WO ₄ nanorods decorated with AgI nanoparticles: Novel and efficient visible-light-driven photocatalysts for the degradation of water pollutants. Beilstein Journal of Nanotechnology, 2018, 9, 1308-1316.	1.5	22
65	Constructing Ag decorated ZnS1-x quantum dots/Ta2O5-x nanospheres for boosted tetracycline removal: Synergetic effects of structural defects, S-scheme heterojunction, and plasmonic effects. Journal of Colloid and Interface Science, 2022, 623, 1085-1100.	5.0	21
66	Spatial Heterogeneity in the Determinants of Urban Form: An Analysis of Chinese Cities with a GWR Approach. Sustainability, 2019, 11, 479.	1.6	20
67	Synthesis of Flower-Like AgI/BiOCOOH p-n Heterojunctions With Enhanced Visible-Light Photocatalytic Performance for the Removal of Toxic Pollutants. Frontiers in Chemistry, 2018, 6, 518.	1.8	18
68	A facile one-pot and alkali-free synthetic procedure for binary SnO2/g-C3N4 composites with enhanced photocatalytic behavior. Materials Science in Semiconductor Processing, 2020, 115, 105112.	1.9	18
69	Construction of Au and C60 quantum dots modified materials of Institute Lavoisier-125(Ti) architectures for antibiotic degradation: Performance, toxicity assessment, and mechanistic insight. Journal of Colloid and Interface Science, 2022, 623, 417-431.	5.0	18
70	Enhanced visible-light photocatalytic activity of Ag/AgI coupled Bi2O2CO3 microspheres. Materials Letters, 2017, 191, 123-127.	1.3	17
71	Hierarchical heterostructures of Bi2MoO6 microflowers decorated with Ag2CO3 nanoparticles for efficient visible-light-driven photocatalytic removal of toxic pollutants. Beilstein Journal of Nanotechnology, 2018, 9, 2297-2305.	1.5	15
72	Controllable Hydrothermal Synthesis and Photocatalytic Performance of Bi2MoO6 Nano/Microstructures. Catalysts, 2020, 10, 1161.	1.6	15

#	Article	IF	CITATIONS
73	Flower-like MWCNTs/Bi2O2CO3 composites with enhanced photocatalytic activity under simulated solar light irradiation. Materials Letters, 2016, 185, 50-53.	1.3	14
74	Ag2CO3 Decorating BiOCOOH Microspheres with Enhanced Full-Spectrum Photocatalytic Activity for the Degradation of Toxic Pollutants. Nanomaterials, 2018, 8, 914.	1.9	14
75	A novel and facile procedure to decorate Bi2O3 with Bi2S3 nanocrystals: Composites synthesis, analyses, and photocatalytic performance assessment. Colloids and Surfaces A: Physicochemical and Engineering Aspects, 2021, 610, 125640.	2.3	14
76	A Novel Flower-Like Ag/AgCl/BiOCOOH Ternary Heterojunction Photocatalyst: Facile Construction and Its Superior Photocatalytic Performance for the Removal of Toxic Pollutants. Nanomaterials, 2019, 9, 1562.	1.9	13
77	Facile Synthesis of Bi2MoO6 Microspheres Decorated by CdS Nanoparticles with Efficient Photocatalytic Removal of Levfloxacin Antibiotic. Catalysts, 2018, 8, 477.	1.6	11
78	3D structured TiO ₂ -based aerogel photocatalyst for the high-efficiency degradation of toluene gas. New Journal of Chemistry, 2022, 46, 2272-2281.	1.4	10
79	Facile Fabrication of Flower-Like BiOI/BiOCOOH p–n Heterojunctions for Highly Efficient Visible-Light-Driven Photocatalytic Removal of Harmful Antibiotics. Nanomaterials, 2019, 9, 1571.	1.9	7